

## Phase-transition induced optimization on electrostrain, electrocaloric refrigeration and energy storage of LiNbO<sub>3</sub> doped BNT-BT ceramics

Yueming Zhang<sup>§1,2</sup>, Guochuang Liang<sup>1,2§</sup>, Silin Tang<sup>1,2§</sup>, Biaolin Peng<sup>1,2\*</sup>,

Qi Zhang<sup>1</sup>, Laijun Liu<sup>3\*</sup>, Wenhong Sun<sup>2\*</sup>

<sup>1</sup>Department of Manufacturing and Materials, Cranfield University, Cranfield, Bedfordshire, MK43 0AL, United Kingdom

<sup>2</sup>Center on Nanoenergy Research, School of Physical Science & Technology, Guangxi University, Nanning 530004, China

<sup>3</sup>Key Laboratory of Nonferrous Materials and New Processing Technology, Ministry of Education, College of Materials Science and Engineering, Guangxi Universities Key Laboratory of Non-ferrous Metal Oxide Electronic Functional Materials and Devices, Guilin University of Technology, Guilin 541004, People's Republic of China

\*Correspondence to: [pengbl8@126.com](mailto:pengbl8@126.com), [ljlju2@163.com](mailto:ljlju2@163.com), [20180001@gxu.edu.cn](mailto:20180001@gxu.edu.cn)

§These authors contributed equality to this work.

### Abstract:

$((\text{Bi}_{0.5}\text{Na}_{0.5}\text{TiO}_3)_{0.88}-(\text{BaTiO}_3)_{0.12})_{(1-x)}-(\text{LiNbO}_3)_x$  ( $x = 0.0, 0.01, 0.02, 0.03, 0.04, 0.05, 0.06, \text{ and } 0.07$ ; abbreviated as LiNbO<sub>3</sub>-doped BNT-BT) ceramics possessing many excellent performances (large electrostrain, negative electrocaloric effect and energy storage density with high efficiency) was fabricated by the conventional solid-state reaction method. A large electrostrain (maximum  $\sim 0.34\%$  at 100 kV/cm and room temperature) with high thermal stability over a broad temperature range ( $\sim 80$  K) is obtained at  $x = 0.03$ . A large energy storage density (maximum  $W_{\text{energy}} \sim 0.665$  J/cm<sup>3</sup> at 100 kV/cm and room temperature) with a high efficiency ( $\eta \sim 49.3\%$ ) is achieved at  $x = 0.06$ . Moreover, a large negative electrocaloric ( $EC$ ) effect (maximum  $\Delta T \sim 1.71$  K with  $\Delta S \sim -0.22$  J/(K kg) at 70 kV/cm) is also obtained at  $x = 0.04$ . Phase transition (from ferroelectric to antiferroelectric and then to relaxor) induced by increasing the doping amount of LiNbO<sub>3</sub> plays a very key role on the optimization of these performances. These findings and breakthroughs make the LiNbO<sub>3</sub>-doped BNT-BT ceramics very promising candidates as multifunctional materials.

Key words: Phase-transition; electrostrain; energy storage; electrocaloric effect

## 1. Introduction

Piezoceramics are a kind of very important functional materials, which have been applied in every corner of human life and production [1-3]. Traditional piezoelectric ceramics are mainly  $\text{PbZrTiO}_3$  (PZT) based binary and ternary ceramics with a series of excellent properties [4,5]. However, these PZT-based piezoelectric ceramics emit toxic substances in the process of preparation and use, causing harm to human body and environment. Therefore, the research and development of lead-free piezoelectric ceramics is an urgent and significant social and economic task.

Bismuth titanate (BNT) lead-free piezoelectric ceramics were discovered in 1960. It was first synthesized by Smolensk et al. which is a kind of composite perovskite ferroelectrics occupied by sodium ions and bismuth ions at position A site [6]. Among thousands of perovskite structures at the position A, BNT is one of the few stable composite perovskite structures. BNT is a triangular symmetric crystal system at room temperature. At about  $230^\circ\text{C}$ , it is transformed into an anti-ferroelectric phase through diffusion phase transformation into a tetragonal phase, and BNT is a cubic phase above  $520^\circ\text{C}$  [7]. BNT ceramic has many advantages, such as strong ferroelectric property [8], good piezoelectric property, small dielectric constant and good acoustic property. The material has broad application prospects, such as high frequency filter, transducer ultrasonic transducer, industrial flaw detection thickness measurement, medical ultrasonic diagnosis and other piezoelectric elements, however, it is difficult to be polarized in ferroelectric phase region due to the large coercive electric field ( $E = 73 \text{ kV/cm}$ ) of pure BNT ceramics, and the sintering temperature range of pure BNT is narrow, so the ceramic compactness is poor[9]. Therefore, it is difficult for pure BNT ceramics to be applied. The key to its application is to improve the piezoelectric activity of BNT and reduce the difficulty of polarization, thus doping is an effective method to get rid of the disadvantages. Takenaka [10] and Chu [11] et al. had done much research work on the BNT-BT system, including the dielectric, piezoelectric and ferroelectric properties, Kumara's[12] improved dielectric systems because of their relatively low response of electrocaloric effect (ECE) as compared to other candidates.

Although there is a steady stream of sporadic progress was made on BNT-BT system coming about[13-18], there never exists a series research on the doped BNT-BT system, ranging from microstructure to macro-properties, including ferroelectric properties, electrostrain, electrocaloric effect and even the energy storage performance. Therefore, this research is based on the LiNbO<sub>3</sub>-doped BNT-12BTceramics prepared by the conventional solid-state reaction method, explaining the mechanism behind the macro performance systematically from the microcosmic point of view, which will make contributions to the further optimization and wider application.

## **2. Experimental process**

### **2.1 Fabrication**

LiNbO<sub>3</sub>-doped BNT-BT ceramics were prepared by the conventional solid-state reaction method. BaCO<sub>3</sub> (purity ≥ 99%), Nb<sub>2</sub>O<sub>5</sub> (purity ≥ 99.99%), Li<sub>2</sub>CO<sub>3</sub> (purity ≥ 98%), Na<sub>2</sub>CO<sub>3</sub> (purity ≥ 99.8%), Bi<sub>2</sub>O<sub>3</sub> (purity ≥ 99%) and TiO<sub>2</sub> (purity ≥ 98%) were used as starting reagents. Bi<sub>2</sub>O<sub>3</sub>, Li<sub>2</sub>CO<sub>3</sub> and Na<sub>2</sub>CO<sub>3</sub> with 3% excess were added due to the volatility of Bi, Li and Na elements. The raw reagents were firstly milled for 12 h by using zirconia balls as media in ethanol. The subsequent slurries were dried and calcined at 850 °C for 6 h, and then the ceramic powders were milled again for another 12 h to minimize the segregation. After further drying and sieving, the ceramic powders were cold-isostatically pressed into pellets with a diameter of ~ 5 mm and a thickness of ~ 1 mm at 300 MPa for 5 min. Subsequently, the pellets were immediately sintered at 1140 °C - 1150 °C for 6 h at a heating rate of 3 °C/min, and then cooled to 800 °C at a cooling rate of 3 °C/min, and finally cooled to room temperature naturally.

### **2.2 Characterization**

The densities of LiNbO<sub>3</sub>-doped BNT-BT ceramics were measured by the Archimedean drainage method. The phase structures of ceramics were analyzed by the X-ray diffraction (XRD, PANalytical X'Pert PRO)

using Cu K $\alpha$  radiation ( $\lambda = 1.5406 \text{ \AA}$ ). The microstructures of ceramics were identified by the field emission scanning electron microscopy (SEM, Pro X, Phenom, Eindhoven, Netherlands). To characterize the electric properties, the sintered samples were polished down to a thickness of 0.5 mm and baked with Ag electrode at 600 °C. The dielectric properties were measured by using a precision impedance analyzer (HP 4192A). The hysteresis loops between the polarizations and electric fields (*P-E loops*) were measured at 1 Hz by using a ferroelectric analyzer (TF-2000, AixACCT, Aachen, Germany).

### 3. Results and discussions

#### 3.1 Structure

**Fig. 1b)** shows the XRD patterns of LiNbO<sub>3</sub>-doped BNT-BT ceramics. All samples exhibit pure perovskite structure after sintering at 1150 °C for 6 h and pyrochlore phase is hard to be detected. For  $x = 0$ , the splitting of peaks ((003) and (021)) at 39.8° doesn't look obvious for all samples. However, the splitting of peaks ((002) and (200)) at 46.6° is very obvious and the gap between them is very large. The (002) diffraction peaks shifted to a higher angle and the corresponding intensity become weaker with the increase of the doping amount of LiNbO<sub>3</sub>, meanwhile, the (200) diffraction peaks shifted to a lower angle with the increase of the doping amount of LiNbO<sub>3</sub> and the gap become narrower, especially at  $x = 0.03$ , where the two peaks have almost merged with each other, indicating that the decrease of the amount of the tetragonal phase (P4mm) with lamellar domain and the increase of the amount of the tetragonal phase (P4bm) with nanodomain. These results indicate that the doping amount of LiNbO<sub>3</sub> play a key role on the phase transition of the structure of BNT-BT ceramics.

**Fig. 2** shows the surface SEM images of LiNbO<sub>3</sub>-doped BNT-BT ceramics etched at 1100 °C for 6 h after polishing mechanically. The grain size of the ceramic decreases sharply with the addition of tiny doping amount ( $x = 0.01$ ) of LiNbO<sub>3</sub>, and the corresponding average grain size ( $\sim 1.96 \mu\text{m}$ ) obtained from the statistical distribution diagram (insets of **Fig.2a**) and **Fig.2b**) has been reduced to the half of one ( $\sim 3.74$

$\mu\text{m}$ ) at  $x = 0$ . With the further addition of  $\text{LiNbO}_3$ , the average grain size keeps almost unchanged, as shown in the insets of **Fig.2c**) to **Fig.2h**). One possible reason for this phenomenon is that the mechanism of densification during the sintering process has been changed from the simple solid-phase-reaction diffusion into a complex one assisted by the liquid phase due to the addition of lithium element with low melting point. As a result, more homogeneous and dense microstructures which benefit to improve the insulation of ceramics and also to reduce the leakage current were obtained after doping by  $\text{LiNbO}_3$ .

### 3.2 Ferroelectric and dielectric properties

**Fig. 3** shows the  $P$ - $E$  hysteresis loops of  $\text{LiNbO}_3$ -doped BNT-BT ceramics and the corresponding current-electric field ( $I$ - $E$ ) curves (insets of **Fig. 3**) at selected electric fields and at 1 Hz. The ceramics with a lower doping amount of  $\text{LiNbO}_3$  ( $x = 0.01$  and  $0.02$ ) including the pure one behaves as typical normal ferroelectrics with single  $P$ - $E$  hysteresis loops. With the further addition of  $\text{LiNbO}_3$ , the ceramic ( $x = 0.03$ ) behaves as a typical antiferroelectrics with double  $P$ - $E$  hysteresis loops (**Fig. 3d**) and four current peaks can be observed obviously on the corresponding  $I$ - $E$  curve, as guided by 1, 2, 3 and 4 in the inset of **Fig. 3 d**). As the doping amount of  $\text{LiNbO}_3$  continues to increase, ceramics behave as typical relaxors with slim  $P$ - $E$  loops, and the four current peaks get more and more blurred, as shown in the insets of **Fig. 3e**), **3f**), **3g**) and **3h**). It is well known that the tolerance factor ( $t = (R_A + R_O) / \sqrt{2} (R_B + R_O)$ ) can be employed to characterize the stability of the  $\text{ABO}_3$  perovskite structure, whose values are usually between 0.77 and 1.1. Generally, the antiferroelectric phase is more readily available as the value of  $t$  is less than 1. It can be seen that the value of  $t$  of  $\text{LiNbO}_3$ -doped BNT-BT ceramics decreases almost linearly with the increase of  $x$  (see the red fitting solid line in the inset of **Fig.3d**). Therefore, the appearance of antiferroelectrics ceramics at a higher doping amount of  $\text{LiNbO}_3$  (especially at  $x = 0.03$ ) is reasonable structurally.

### 3.3 Electrostrain property

**Fig. 4** shows the variable temperature electrostrain curve ( $S$ - $E$ ) of  $(1-x)$  (BNT-12BT)- $x$ LiNbO<sub>3</sub> ceramic samples. The electrostrain of ceramics with different doping amount have obvious different characteristics, the change of the LiNbO<sub>3</sub> doping amount obviously influences the value of the electrostrain, the undoped ceramic sample has an obvious ferroelectric property in a butterfly-shape with both positive and negative electrostrain at room temperature but changes to a leaf-bud shape with only a positive electrostrain as the amount increases. Meanwhile, it can be found that the electrostrain curve of variable temperature does not change obviously with the change of temperature at first, but when the amount of doping  $x=2\%$ , the change of temperature has a great influence on the electrical properties of the sample, and the sample exhibits excellent stability and pretty high quality when  $x=3\%$ . With the increase of temperature, the change of shapes can be attributed to the transformation of the sample from the ferroelectric phase at room temperature to the short-range ordered relaxor phase under the condition of thermal activation. This temperature-induced phase transition can be more and more beam waist corresponding to the ferroelectric pattern of the sample with the increase of temperature in the variable temperature ferroelectric. To make a further comparison, the electrostrain curves of  $(1-x)$  (BNT-12BT)- $x$ LiNbO<sub>3</sub> ceramic sample ( $S$ - $E$ ) at selected electric fields are shown in **Fig. S3**. The value of the electrostrain is proportional to the intensity of the applied electric field with the doping amount always served as the key factor. The electrostrain increases with the adding of doping amount at first, and then reaches the maximum value of about 0.34% when  $x = 3\%$ , which is obviously higher than that of pure ceramic samples. While, if the doping amount continues to rise, the electrostrain of ceramic samples decreases on the contrary, which means moderate LiNbO<sub>3</sub> doping is beneficial to enhance the electrostrain of the system, exhibiting excellent properties near the morphotropic phase boundary (MPB) with a giant electrostrain. Combined with its ferroelectric properties, it turns out that the negative electrostrain was formed by the reversal of ferroelectric domain in ceramic under electric field rather than by antiferroelectric and relaxor ferroelectric, which is consistent with the phase transition shown

in the previous dielectric temperature spectrum and current diagram. Besides, the relationship curve of electrostriction and polarization square ( $S-P^2$ ) of (1-x)(BNT-12BT)-xLiNbO<sub>3</sub> ceramic samples is also concluded in **Fig. S4**, it can be seen that the electrostrictive coefficient  $Q$  varies little with the electric field, but the electrostrictive coefficient  $Q$  varies greatly with doping. The electrostrictive coefficient  $Q$  of ceramics increases at first and then decreases, the deviation may be due to the negative pressure electric effect. Electrostriction is proportional to the square of the polarization, as shown in the **Equation (1)**:

$$S = QP^2 \quad (1)$$

Where  $Q$  is the electrostrictive coefficient and  $P$  is the polarization intensity. The electric field dependence of (1-x) (BNT-12BT)-xLiNbO<sub>3</sub> ceramic electrostrictive coefficient  $Q$  is obtained by fitting the  $S-P^2$  curve. It can be seen that the  $S-P^2$  curve are basically linear, especially the doping amount  $x = 0.06$  under 80kV/cm electric field, showing the best linearity and the maximum  $Q = 0.04154\text{m}^4/\text{C}^2$ , which is much higher than the previous report ( $0.0254 \text{ m}^4/\text{C}^2$ )[30].

### 3.4 Energy storage performance

**Fig. 5** shows the relationship between energy storage density ( $W_{\text{energy}}$ ), efficiency ( $\eta$ ), energy storage loss ( $W_{\text{loss}}$ ) and electric field intensity of (1-x)(BNT-12BT)-xLiNbO<sub>3</sub> ceramic samples. The recoverable energy density ( $W_{\text{energy}}$ ) of a dielectric-based material is estimated from the  $P$ - $E$  loops and calculated with the following **Equation (2) and (3)**

$$W = \int_{P_r}^{P_{\text{max}}} E dP \quad (2)$$

$$\eta = \frac{W_{\text{energy}}}{W_{\text{energy}} + W_{\text{loss}}} \times 100\% \quad (3)$$

where  $E$  is the applied electric field that causes variation in the electric polarization  $P$ ,  $P_r$  the remnant polarization, and  $P_{\text{max}}$  the maximum polarization under the applied field[31, 32]. According to **Equation (2)**, materials possessing smaller  $P_r$ , larger  $P_{\text{max}}$ , and higher dielectric breakdown strength simultaneously are more favorable for energy storage. For practical applications, in addition to a large  $W_{\text{energy}}$ , the high energy

storage efficiency ( $\eta$ ) is also desired, which is defined as the ratio of the discharging (output) energy to the charging (input) energy. It can be seen that the energy storage density and loss of all samples increase with the added electric field. The energy storage efficiency does not change obviously with the variation of electric fields. With the increase of doping amount, the energy storage density and energy storage loss increase continuously, reaching the maximum value of  $W_{\text{energy}} = 0.665 \text{ J/cm}^3$  and  $\eta = 49.3\%$  when the doping amount is  $x = 0.06$  at the  $100 \text{ kV/cm}$  applied electric field. The energy storage loss is continuously decreased with the increase of doping amount. At the doping amount  $x = 0.06$ , the energy storage loss is controlled at about  $10\%$ . In addition, where the linearity of energy storage density and efficiency is pretty good and shows an upward trend. Although the energy storage density at this time is not very high compared with the highest value provided by the peer, which comes from the samples prepared on a larger and thinner substrate[33, 34], however, the samples we made is fabricated on the substrate with larger and thicker substrate. If the area of the electrode and the thickness of sample could be decreased, the energy storage density of the material would be greatly enhanced according to the linear trend as shown in the data, which will be far more giant than the existing energy storage value.

### 3.5 Electrocaloric effect

**Fig. 6** shows the change of temperature and entropy tested at  $1\text{Hz}$  at selected electric fields, it can be found that when  $x$  shows a relative high negative electrocaloric effect but unstable. The Maxwell relational expression  $(\partial P/\partial T)_E = (\partial S/\partial E)_T$  is assumed to be valid under the condition of reversible adiabatic approximation. The *EC* effect of La doped BNT-6BT ceramics can be obtained from **Equation (4) and (5)**.

$$\Delta T = -\frac{1}{\rho} \int_{E_1}^{E_2} \left( \frac{T}{C} \right) \left( \frac{\partial P}{\partial T} \right) E dE \quad (4)$$

$$\Delta S = -\frac{1}{\rho} \int_{E_1}^{E_2} \left( \frac{\partial P}{\partial T} \right) E dE \quad (5)$$

In **Equation (2) and (3)**,  $P$  is the maximum polarization at the applied electric field  $E$ ,  $T$  the operating temperature, and  $E_1$  and  $E_2$  the initial and final applied electric field respectively[35]. With the increase of



doping amount, the tendency of the curve shows an obvious regularity: the higher electric fields and temperature make contributions to the larger  $EC$ , especially when the doping amount  $x = 4\%$ , the sample exhibits the best electrocaloric property at the 70 kV/cm electric field ( $\Delta T = -1.71$  K,  $\Delta S = -2.1519$  J/(K·kg)). The similar results are also confirmed by the temperature-varying hysteretic loops at the 70 kV/cm electric field (**Fig. S2**), and each hysteretic loop is tested every 10 K for the same sample. It clearly emerges that when  $x=4\%$ , the degree of coincidence of the curve is the slightest, indicating that the ferroelectric property is the most unstable affected by the temperature change greatly, which is corresponding to electrocaloric patterns referred above. Nevertheless, as the doping amount keeps adding, the electrocaloric effect becomes small reversely. Compared with the patterns in XRD and SEM, it can be inferred that the initial state is due to the little doping, resulting in many defects and voids in the sample with large leakage current, which is unstable and not the intrinsic state of the material. Subsequently, the rising doping amount contributes to the dense, uniform and stable formation of the material, thus exhibiting a strong regularity of the electrocaloric effect. Furthermore, connected with the ferroelectric property (**Fig. 3**) and dielectric temperature spectrum (**Fig. S2**), it can be seen that there exists a phase transition because of the unstable phase structure due to decreasing tolerance factor caused by the  $\text{LiNbO}_3$  adding, which always cause the FE/AFE phase transition, where the giant  $EC$  always lies[36].

## Conclusion

The giant electrostrain effect and energy storage, together with series pretty good properties have been achieved by the  $\text{LiNbO}_3$ -doped BNT-BT fabricated by a conventional solid-state reaction method with the change of doping amount. It can be concluded that the  $\text{LiNbO}_3$ -doping will cause an AFE/FE transition due to the phase transition from rhombohedral to tetragonal, which always brings about a giant negative  $EC$ , the ferroelectric and anti-ferroelectric properties, along with a more diffuse dispersion around the dielectric, resulting in a broader operational temperature range. The stable performance of the giant electrostriction, especially when  $x = 3\%$  allows the material to a keep steady performance even if the temperature varies. The

energy storage capacity exhibits a linear upwards tendency, indicating that the capacity will continue to increase with the higher electric field provided. Combined with so many optimized features resulted from the LiNbO<sub>3</sub> doping strategy, it makes a possibility for LiNbO<sub>3</sub>-doped BNT-BT system to become a more potential and wide-applied material in the near future.

### Acknowledgement

This work was supported by the National Natural Science Foundation of China (51402196), the Guangxi Natural Science Foundation (Grants 2016GXNSFCB380006, 2017GXNSFFA198015).

### Reference

- [1] J. Anthoniappen, C. S. Tu, P. Y. Chen, C. S. Chen, S. J. Chiu, H. Y. Lee, *et al.*, "Structural phase stability and electric field induced relaxor-ferroelectric phase transition in  $(1-x)(\text{Bi}_{0.5}\text{Na}_{0.5})\text{TiO}_3-x\text{BaTiO}_3$  ceramics," *Journal of Alloys and Compounds*, vol. 618, pp. 120-126, 2015.
- [2] C. Ma, H. Guo, S. P. Beckman, and X. Tan, "Creation and destruction of morphotropic phase boundaries through electrical poling: a case study of lead-free  $(\text{Bi}_{(1/2)}\text{Na}_{(1/2)})\text{TiO}_3\text{-BaTiO}_3$  piezoelectrics," *Phys Rev Lett*, vol. 109, p. 107602, Sep 7 2012.
- [3] S. Ozaki, S. Matsuyama, M. Sasaki, T. Nakanishi, T. Sugawara, Ieee, *et al.*, "An ultra thin nitrated oxide gate pielectric formation by using slot plane antenna plasma," in *Ascmc 2003: Ieee/Semi*, ed New York: Ieee, 2003, pp. 137-141.
- [4] C. F. Wei and X. J. Jing, "A comprehensive review on vibration energy harvesting: Modelling and realization," *Renewable & Sustainable Energy Reviews*, vol. 74, pp. 1-18, Jul 2017.
- [5] B. Peng, Q. Zhang, X. Li, T. Sun, S. Ke, M. Ye, *et al.*, "High dielectric tunability, electrostriction strain and electrocaloric strength at a tricritical point of tetragonal, rhombohedral and pseudocubic phases," *Journal of Alloys and Compounds*, vol. 646, pp. 597-602, 2015.
- [6] H. Jeong, J. Bao, R. Da, H. Yong, and I. Byung, "The potential application of BNT-based ceramics

- in large displacement actuation," *Journal of Ceramic Processing Research*, vol. 3, pp. 231-234, 2002.
- [7] C. Ma and X. Tan, "Phase diagram of unpoled lead-free ceramics," *Solid State Communications*, vol. 150, pp. 1497-1500, 2010.
- [8] M. Munir, A. Hussain, J. Y. Ock, J. H. Son, S. A. Khan, and D. S. Bae, "Structure Analysis and Ferroelectric Response of  $\text{Bi}_{0.5}\text{Na}_{0.5}\text{TiO}_3$  Nanopowder Synthesized by Sol-Gel Method," *Journal of Nanoscience and Nanotechnology*, vol. 19, pp. 1323-1329, Mar 2019.
- [9] E. Taghaddos, H. Charalambous, T. Tsakalakos, and A. Safari, "Electromechanical properties of flash sintered BNT-based piezoelectric ceramic," *Journal of the European Ceramic Society*, vol. 39, pp. 2882-2888, Aug 2019.
- [10] T. Takenaka, K. Maruyama, and K. Sakata, " $(\text{Bi}_{1/2}\text{Na}_{1/2})\text{TiO}_3$ - $\text{BaTiO}_3$  System for Lead-Free Piezoelectric Ceramics," *Japanese Journal of Applied Physics*, vol. 30, pp. 2236-2239, 2014.
- [11] B. J. Chu, G. R. Li, Q. R. Yin, W. Z. Zhang, and D. R. Chen, "Influence of nonstoichiometry and doping on electrical properties of  $(\text{Na}_{1/2}\text{Bi}_{1/2})_{0.92}\text{Ba}_{0.08}\text{TiO}_3$  ceramics," *Acta Physica Sinica*, vol. 50, pp. 2012-2016, 2001.
- [12] S. Kumaragurubaran, T. Nagata, Y. Tsunekawa, K. Takahashi, S.-G. Ri, S. Suzuki, *et al.*, "Epitaxial growth of high dielectric constant lead-free relaxor ferroelectric for high-temperature operational film capacitor," *Thin Solid Films*, vol. 592, p. S0040609015008470, 2015.
- [13] C. Ma, X. Tan, E. Dul'kin, and M. Roth, "Domain structure-dielectric property relationship in lead-free  $(1-x)(\text{Bi}_{1/2}\text{Na}_{1/2})\text{TiO}_3$ - $x\text{BaTiO}_3$  ceramics," *Journal of Applied Physics*, vol. 108, p. 104105, 2010.
- [14] W. Jo, S. Schaab, E. Sapper, L. A. Schmitt, H.-J. Kleebe, A. J. Bell, *et al.*, "On the phase identity and its thermal evolution of lead free  $(\text{Bi}_{1/2}\text{Na}_{1/2})\text{TiO}_3$ -6mol%  $\text{BaTiO}_3$ ," *Journal of Applied Physics*, vol. 110, p. 074106, 2011.

- [15] B. Wylie-van Eerd, D. Damjanovic, N. Klein, N. Setter, and J. Trodahl, "Structural complexity of  $(\text{Na}_{0.5}\text{Bi}_{0.5})\text{TiO}_3\text{-BaTiO}_3$  as revealed by Raman spectroscopy," *Physical Review B*, vol. 82, p. 104112, 2010.
- [16] X. X. Wang, H. L. W. Chan, and C. L. Choy, " $(\text{Bi}_{0.5}\text{Na}_{0.5})_{0.94}\text{Ba}_{0.06}\text{TiO}_3$  lead-free ceramics with simultaneous addition of  $\text{CeO}_2$  and  $\text{La}_2\text{O}_3$ ," *Applied Physics A*, vol. 80, pp. 333-336, 2005.
- [17] W. Jo, J. E. Daniels, J. L. Jones, X. Tan, P. A. Thomas, D. Damjanovic, *et al.*, "Evolving morphotropic phase boundary in lead-free  $(\text{Bi}_{1/2}\text{Na}_{1/2})\text{TiO}_3\text{-BaTiO}_3$  piezoceramics," *Journal of Applied Physics*, vol. 109, p. 014110, 2011.
- [18] C. Xu, D. Lin, and K. W. Kwok, "Structure, electrical properties and depolarization temperature of  $(\text{Bi}_{0.5}\text{Na}_{0.5})\text{TiO}_3\text{-BaTiO}_3$  lead-free piezoelectric ceramics," *Solid State Sciences*, vol. 10, pp. 934-940, 2008.
- [19] L. Li, M. Xu, Q. Zhang, P. Chen, N. Wang, D. Xiong, *et al.*, "Electrocaloric effect in La-doped BNT-6BT relaxor ferroelectric ceramics," *Ceramics International*, vol. 44, pp. 343-350, 2018.
- [20] X. Wang, H. L.-W. Chan, and C.-l. Choy, "Piezoelectric and dielectric properties of  $\text{CeO}_2$ -added  $(\text{Bi}_{0.5}\text{Na}_{0.5})_{0.94}\text{Ba}_{0.06}\text{TiO}_3$  lead-free ceramics," *Solid State Communications*, vol. 125, pp. 395-399, 2003.
- [21] W. Jo and J. r. Roì?del, "Electric-field-induced volume change and room temperature phase stability of  $(\text{Bi}_{1/2}\text{Na}_{1/2})\text{TiO}_3\text{-x mol. % BaTiO}_3$  piezoceramics," *Applied Physics Letters*, vol. 99, p. 2236, 2011.
- [22] P.-Y. Chen, C.-S. Chen, C.-S. Tu, P.-H. Chen, and J. Anthoniappen, "Effects of texture on microstructure, Raman vibration, and ferroelectric properties in 92.5%  $(\text{Bi}_{0.5}\text{Na}_{0.5})\text{TiO}_3\text{-7.5% BaTiO}_3$  ceramics," *Journal of the European Ceramic Society*, vol. 36, pp. 1613-1622, 2016.
- [23] I. C. Ho, "Semiconducting Barium Titanate Ceramics Prepared by Boron-Containing Liquid-Phase Sintering," *Journal of the American Ceramic Society*, vol. 77, pp. 829-832, 2010.

- [24] J. S. C. Jang, J. C. Fwu, L. J. Chang, G. J. Chen, and C. T. Hsu, "Study on the solid-phase sintering of the nano-structured heavy tungsten alloy powder," *Journal of Alloys & Compounds*, vol. 434, pp. 367-370, 2007.
- [25] Y. E. Geguzin and Y. I. Klinchuk, "Mechanism and kinetics of the initial stage of solid-phase sintering of compacts from powders of crystalline solids (sintering "activity")," *Soviet Powder Metallurgy & Metal Ceramics*, vol. 15, pp. 512-518, 1976.
- [26] Q. Zhang, T. Yang, Y. Zhang, and X. Yao, "Phase transition and electric field induced strain properties in Sm modified lead zirconate stannate titanate based antiferroelectric ceramics," *Journal of Applied Physics*, vol. 113, p. 192901, 2013.
- [27] A. Khesro, R. Boston, I. Sterianou, D. C. Sinclair, and I. M. Reaney, "Phase transitions, domain structure, and pseudosymmetry in La- and Ti-doped BiFeO<sub>3</sub>," *Journal of Applied Physics*, vol. 119, pp. 027602-4846, 2016.
- [28] R. Xu, J. Tian, Z. Xu, Q. Zhu, T. Zhao, Y. Feng, *et al.*, "Effects of La-induced phase transition on energy storage and discharge properties of PLZST ferroelectric/antiferroelectric ceramics," *Ceramics International*, vol. 43, 2017.
- [29] Y. Xu, G. Wang, Y. Tian, Y. Yan, X. Liu, and Y. Feng, "Crystal structure and electrical properties of AgNbO<sub>3</sub>-based lead-free ceramics," *Ceramics International*, vol. 42, p. S027288421631553X, 2016.
- [30] L. Li, M. Zhu, Q. Wei, M. Zheng, Y. Hou, and J. Hao, "Ferroelectric P4mm to relaxor P4bm transition and temperature-insensitive large strains in Bi(Mg<sub>0.5</sub>Ti<sub>0.5</sub>)O<sub>3</sub>-modified tetragonal 0.875Bi<sub>0.5</sub>Na<sub>0.5</sub>TiO<sub>3</sub>-0.125BaTiO<sub>3</sub> lead-free ferroelectric ceramics," *Journal of the European Ceramic Society*.
- [31] Y. H. Huang, Y. J. Wu, J. Li, B. Liu, and X. M. Chen, "Enhanced energy storage properties of barium strontium titanate ceramics prepared by sol-gel method and spark plasma sintering," *Journal of Alloys and Compounds*, vol. 701, pp. 439-446, 2017.

- [32] Q. Hu, L. Jin, T. Wang, C. Li, Z. Xing, and X. Wei, "Dielectric and temperature stable energy storage properties of  $0.88\text{BaTiO}_3\text{-}0.12\text{Bi}(\text{Mg}_{1/2}\text{Ti}_{1/2})\text{O}_3$  bulk ceramics," *Journal of Alloys and Compounds*, vol. 640, pp. 416-420, 2015.
- [33] X. Qi, H. Liu, Z. Lin, M. Cao, J. Xie, H. Hua, *et al.*, "Energy storage properties of BNT-BT based solid solution," in *International Symposium on Applications of Ferroelectric*, 2015.
- [34] G. Viola, H. Ning, M. J. Reece, R. Wilson, T. M. Correia, P. Weaver, *et al.*, "Reversibility in electric field-induced transitions and energy storage properties of bismuth-based perovskite ceramics," *Journal of Physics D Applied Physics*, vol. 45, p. 355302, 2012.
- [35] W. Geng, Y. Liu, X. Meng, L. Bellaiche, J. F. Scott, B. Dkhil, *et al.*, "Giant Negative Electrocaloric Effect in Antiferroelectric La-Doped  $\text{Pb}(\text{ZrTi})\text{O}_3$  Thin Films Near Room Temperature," *Adv Mater*, vol. 27, pp. 3165-9, May 27 2015.
- [36] B. Peng, H. Fan, and Q. Zhang, "A giant electrocaloric effect in nanoscale antiferroelectric and ferroelectric phases coexisting in a relaxor  $\text{Pb}_{0.8}\text{Ba}_{0.2}\text{ZrO}_3$  thin film at room temperature.," *Advanced Functional Materials*, vol. 23, pp. 2987-2992, 2013.

## Figures and Captions

**Figure 1.** a) Phase diagram of the  $(1-x)(\text{Bi}_{1/2}\text{Na}_{1/2})\text{TiO}_3-x\text{BaTiO}_3$  ceramics. PE, AFE, and FE represent paraelectric, antiferroelectric, and ferroelectric phase, respectively. b) XRD patterns of  $(1-x)(\text{BNT-12BT})-x\text{LiNbO}_3$  ceramics.

**Figure 2.** Surface SEM images of  $(1-x)(\text{BNT-12BT})-x\text{LiNbO}_3$  ceramics after thermal etched. a)  $x = 0$ , b)  $x = 0.01$ , c)  $x = 0.02$ , d)  $x = 0.03$ , e)  $x = 0.04$ , f)  $x = 0.05$ , g)  $x = 0.06$  and h)  $x = 0.07$ .

**Figure 3.**  $P$ - $E$  loops of  $(1-x)(\text{BNT-12BT})-x\text{LiNbO}_3$  ceramics at selected electric fields. Insets: the corresponding  $I$ - $E$  curves. a)  $x = 0$ , b)  $x = 0.01$ , c)  $x = 0.02$ , d)  $x = 0.03$ , e)  $x = 0.04$ , f)  $x = 0.05$ , g)  $x = 0.06$  and h)  $x = 0.07$ .

**Figure 4.**  $S_{\text{strain}}(E)$  of  $(1-x)(\text{BNT-12BT})-x\text{LiNbO}_3$  ceramics at selected temperatures, a)  $x = 0$ , b)  $x = 0.01$ , c)  $x = 0.02$ , d)  $x = 0.03$ , e)  $x = 0.04$ , f)  $x = 0.05$ , g)  $x = 0.06$  and h)  $x = 0.07$ .

**Figure 5.**  $W_{\text{energy}}$ ,  $W_{\text{loss}}$ ,  $\eta$  and  $Q$  of  $(1-x)(\text{BNT-12BT})-x\text{LiNbO}_3$  at selected electric fields, a)  $x = 0$ , b)  $x = 0.01$ , c)  $x = 0.02$ , d)  $x = 0.03$ , e)  $x = 0.04$ , f)  $x = 0.05$ , g)  $x = 0.06$  and h)  $x = 0.07$ .

**Figure 6.**  $\Delta T(T)$  of  $(1-x)(\text{BNT-12BT})-x\text{LiNbO}_3$  ceramics at selected electric fields. Insets:  $\Delta S(T)$ . a)  $x = 0$ , b)  $x = 0.01$ , c)  $x = 0.02$ , d)  $x = 0.03$ , e)  $x = 0.04$ , f)  $x = 0.05$ , g)  $x = 0.06$  and h)  $x = 0.07$ .

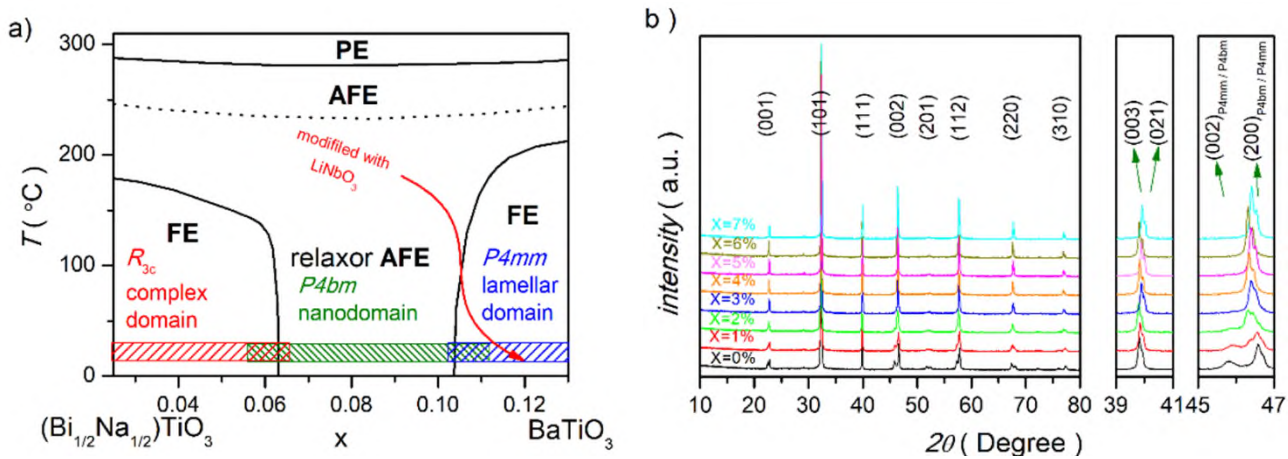


Figure 1



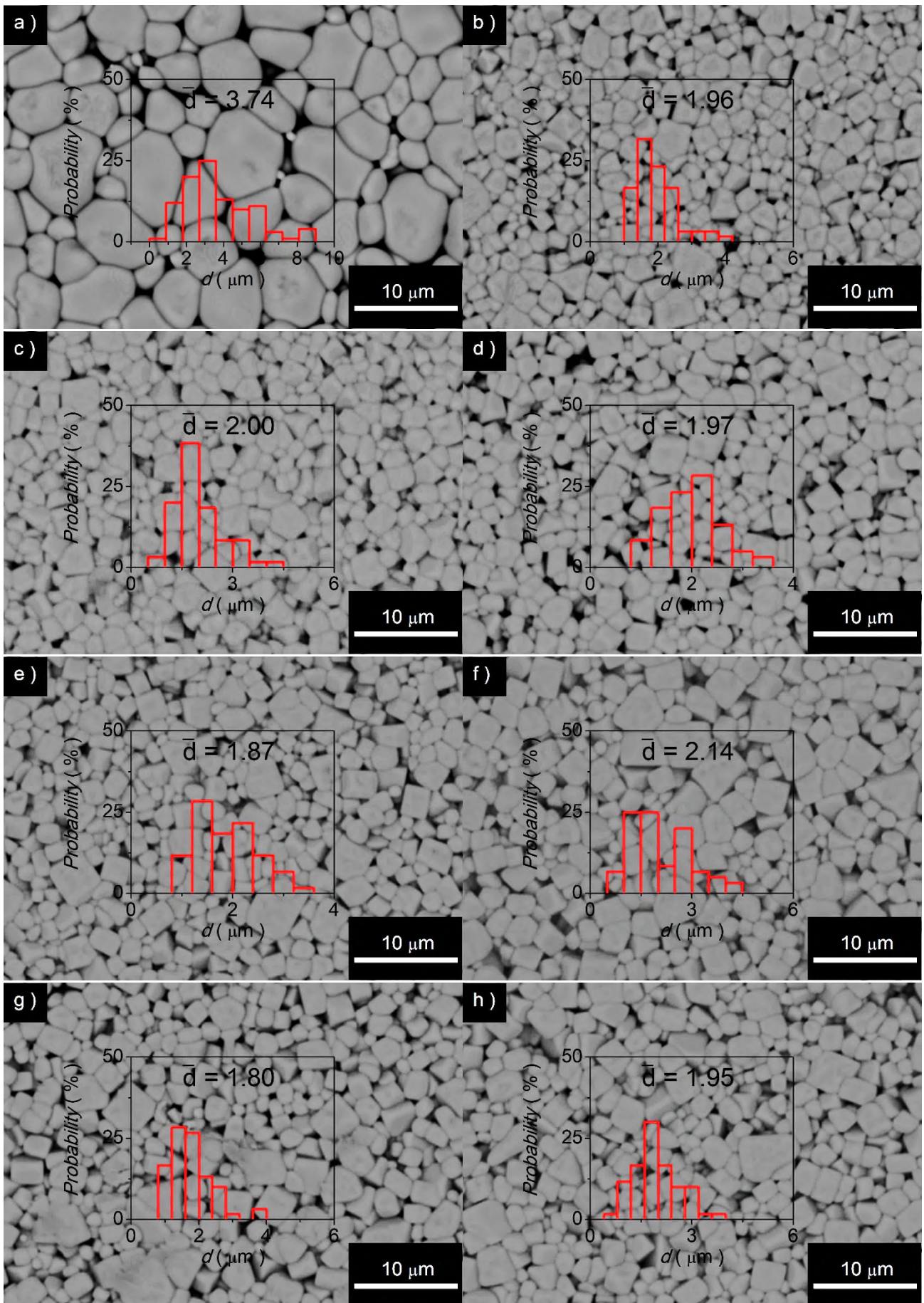


Figure 2

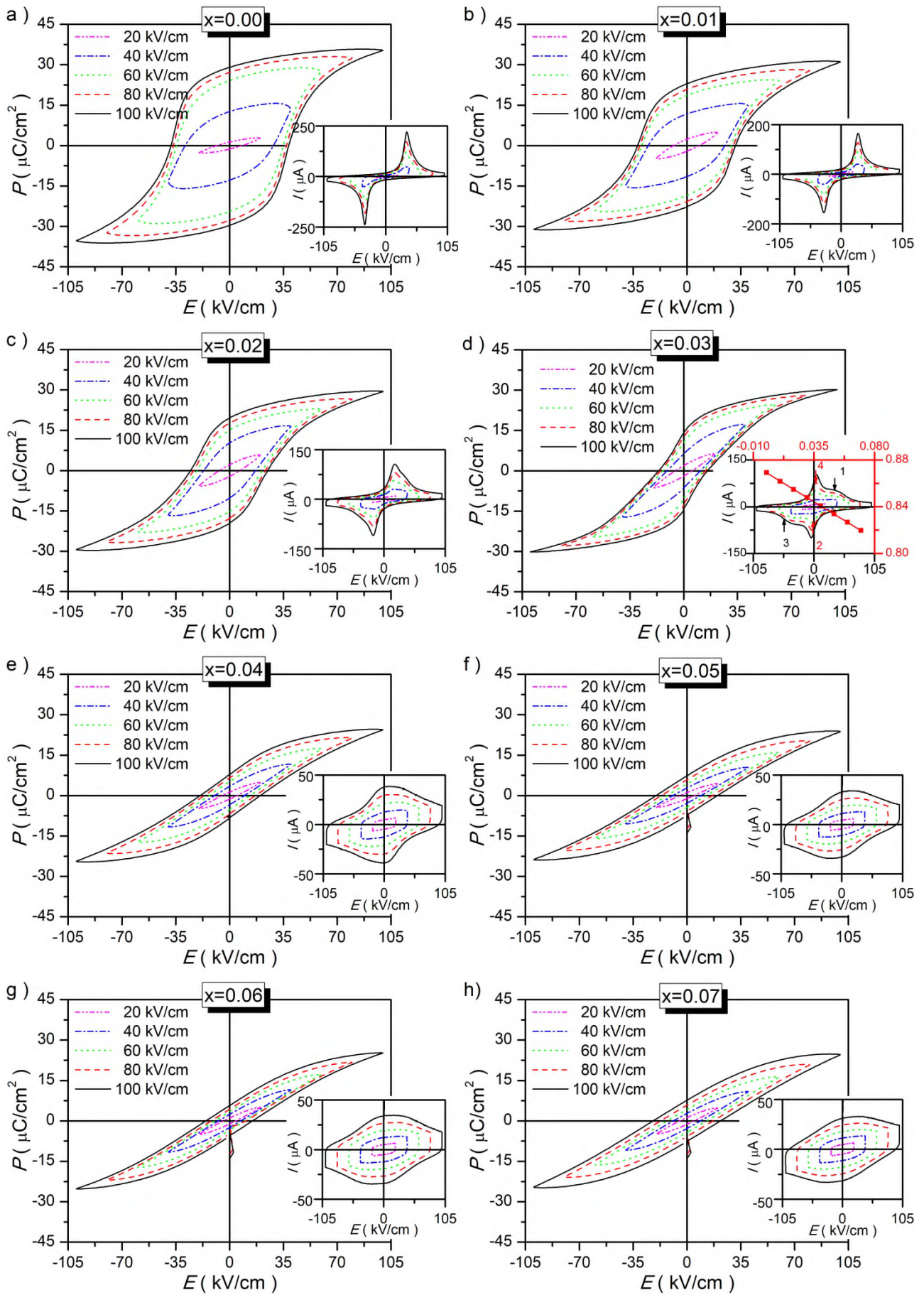
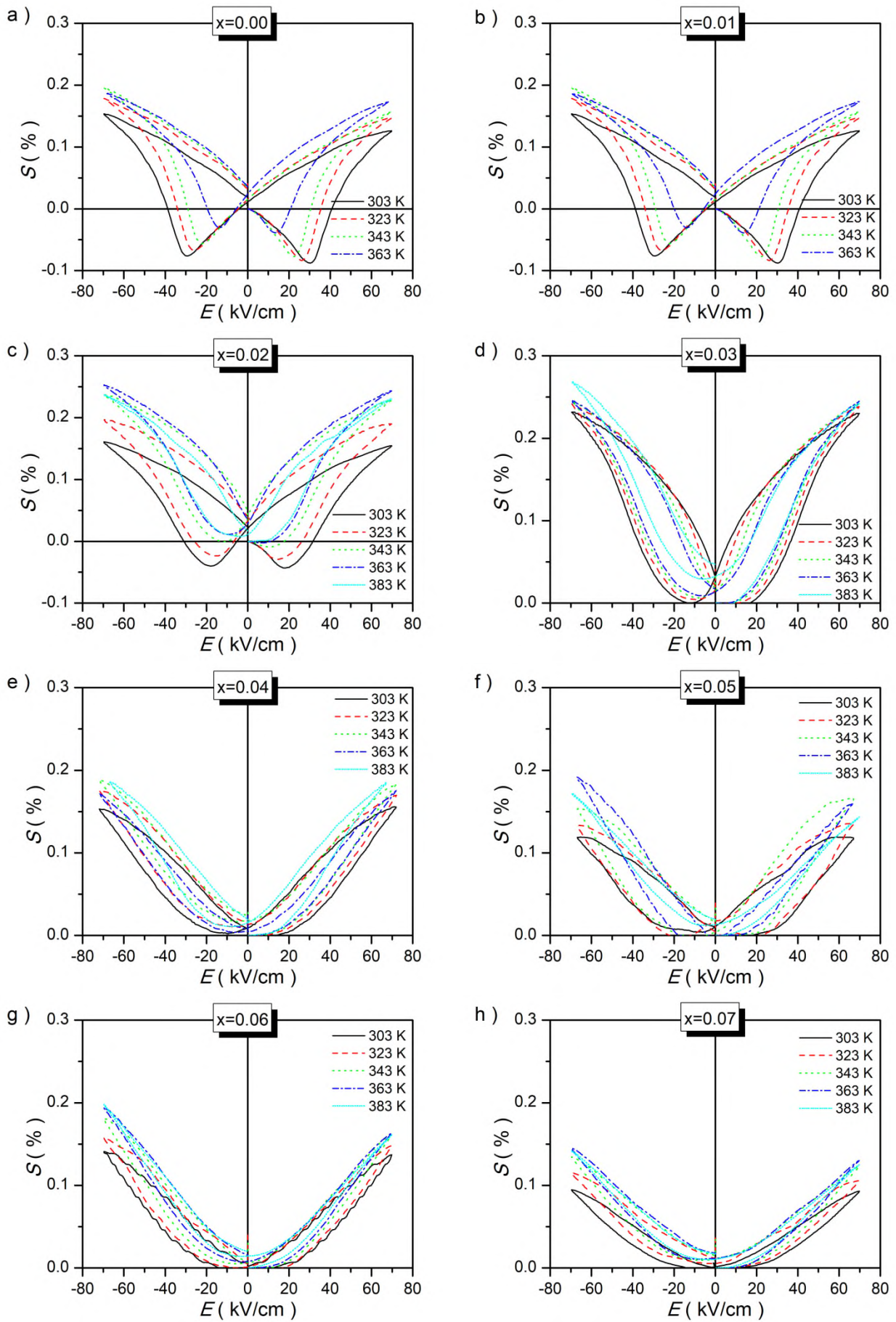
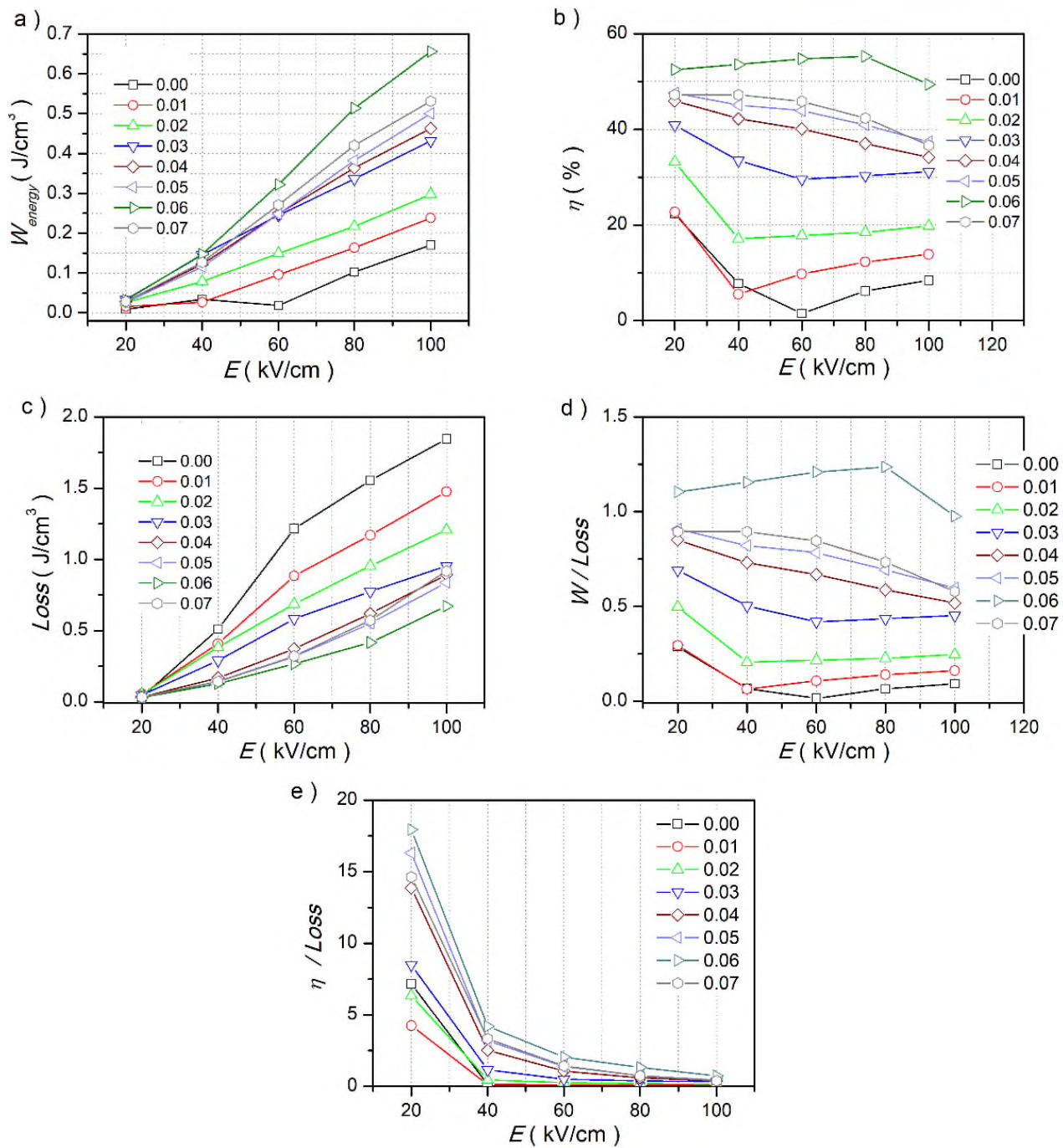


Figure 3



**Figure 4**



**Figure 5**

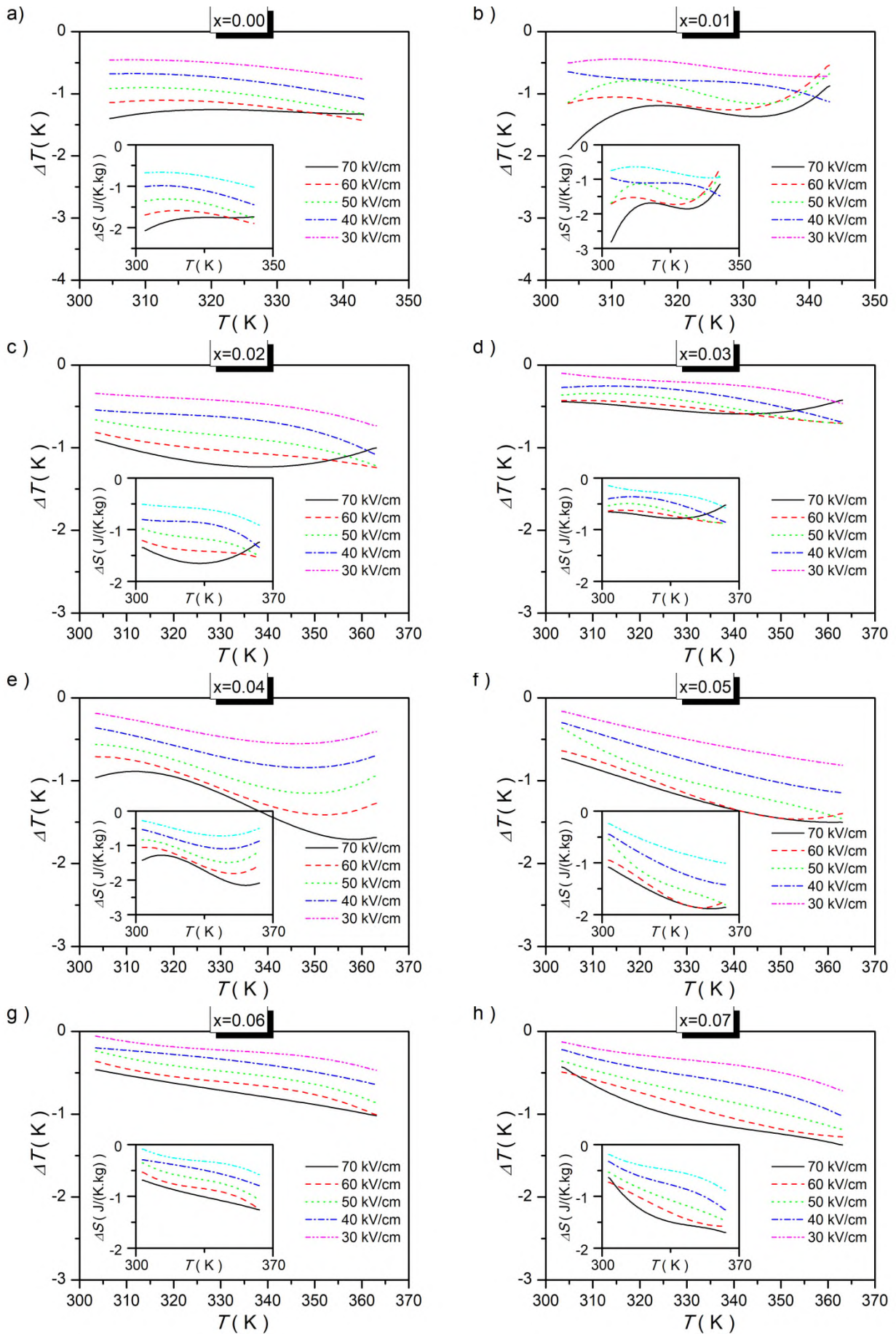


Figure 6

## Supplementary materials for

### **High-performance La-doped BCZT thin film capacitors on LaNiO<sub>3</sub>/Pt composite bottom electrodes with ultra-high efficiency and high thermal stability**

Yueming Zhang<sup>§1,2</sup>, Guochuang Liang<sup>§1,2</sup>, Silin Tang<sup>§1,2</sup>, Bialin Peng<sup>1,2\*</sup>, Qi Zhang<sup>1</sup>, Laijun Liu<sup>3\*</sup>,

Wenhong Sun<sup>2\*</sup>

<sup>1</sup>Department of Manufacturing and Materials, Cranfield University, Cranfield, Bedfordshire, MK43 0AL,  
United Kingdom

<sup>2</sup>Center on Nanoenergy Research, School of Physical Science & Technology, Guangxi University, Nanning  
530004, China

<sup>3</sup>Key Laboratory of Nonferrous Materials and New Processing Technology, Ministry of Education, College  
of Materials Science and Engineering, Guangxi Universities Key Laboratory of Non-ferrous Metal Oxide  
Electronic Functional Materials and Devices, Guilin University of Technology, Guilin 541004, People's  
Republic of China

\*Correspondence to: [pengbl8@126.com](mailto:pengbl8@126.com), [20180001@gxu.edu.cn](mailto:20180001@gxu.edu.cn), [Q.zhang@cranfield.ac.uk](mailto:Q.zhang@cranfield.ac.uk)

This PDF file includes:

Figure S1 to S5

**Figure S1.** Temperature dependence of dielectric permittivity and dielectric loss of (1-x)(BNT-12BT)-xLiNbO<sub>3</sub> ceramics. a) x = 0, b) x = 0.01, c) x = 0.02, d) x = 0.03, e) x = 0.04, f) x = 0.05, g) x = 0.06 and h) x = 0.07.

**Figure S2.** *P-E* loops of (1-x)(BNT-12BT)-xLiNbO<sub>3</sub> ceramics at selected temperatures. a) x = 0, b) x = 0.01, c) x = 0.02, d) x = 0.03, e) x = 0.04, f) x = 0.05, g) x = 0.06 and h) x = 0.07.

**Figure S3.**  $S_{\text{strain}}(E)$  of (1-x)(BNT-12BT)-xLiNbO<sub>3</sub> ceramics at selected electric fields, a) x = 0, b) x = 0.01, c) x = 0.02, d) x = 0.03, e) x = 0.04, f) x = 0.05, g) x = 0.06 and h) x = 0.07

**Figure S4.** Electrostriction diagram of (1-x)(BNT-12BT)-xLiNbO<sub>3</sub> ceramics at selected electric fields, a) x = 0, b) x = 0.01, c) x = 0.02, d) x = 0.03, e) x = 0.04, f) x = 0.05, g) x = 0.06 and h) x = 0.07

**Figure S5.**  $\partial P/\partial T(T)$  of (1-x)(BNT-12BT)-xLiNbO<sub>3</sub> ceramics at selected electric fields. Insets: *P(T)*. a) x = 0, b) x = 0.01, c) x = 0.02, d) x = 0.03, e) x = 0.04, f) x = 0.05, g) x = 0.06 and h) x = 0.07.

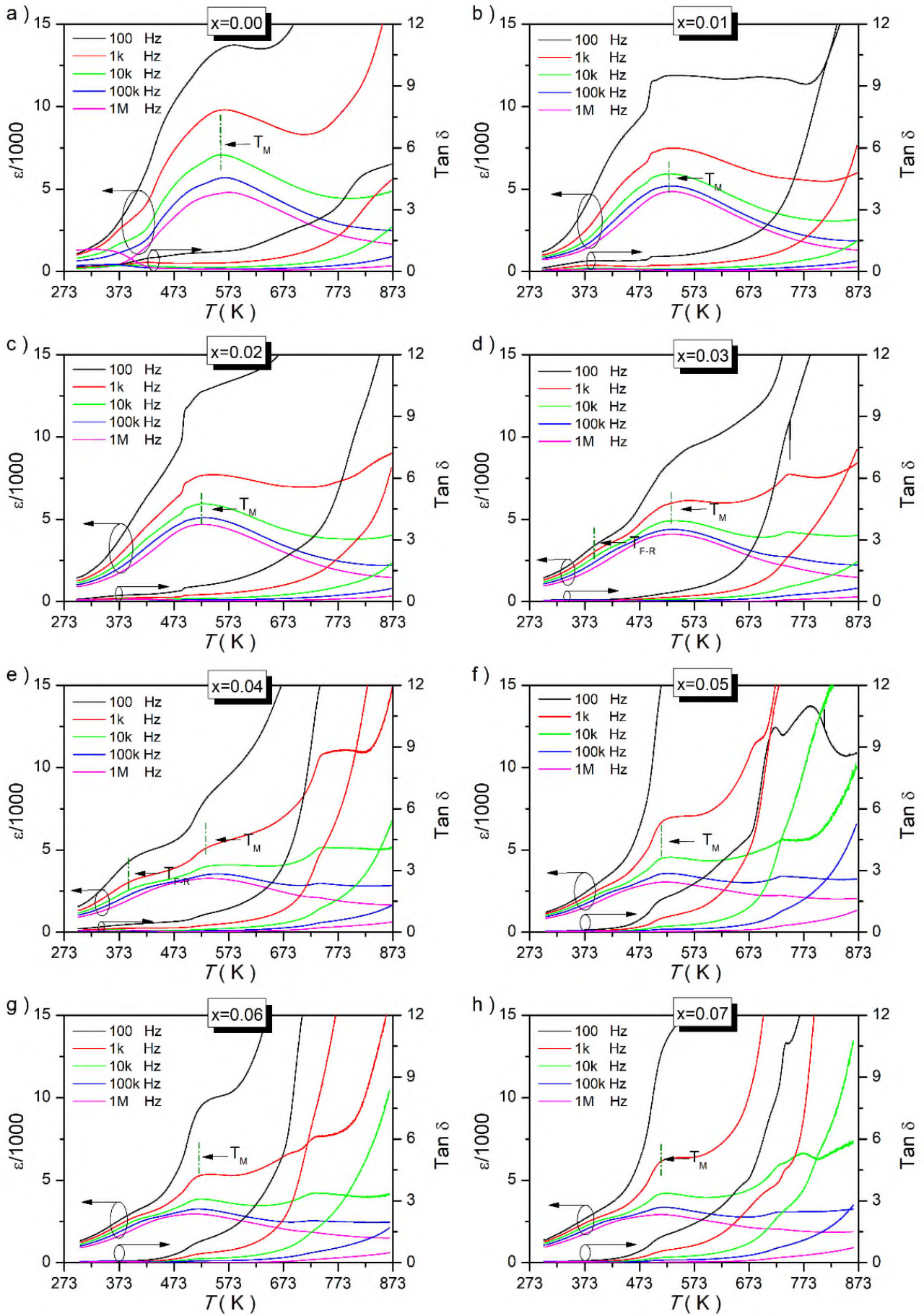


Figure S1



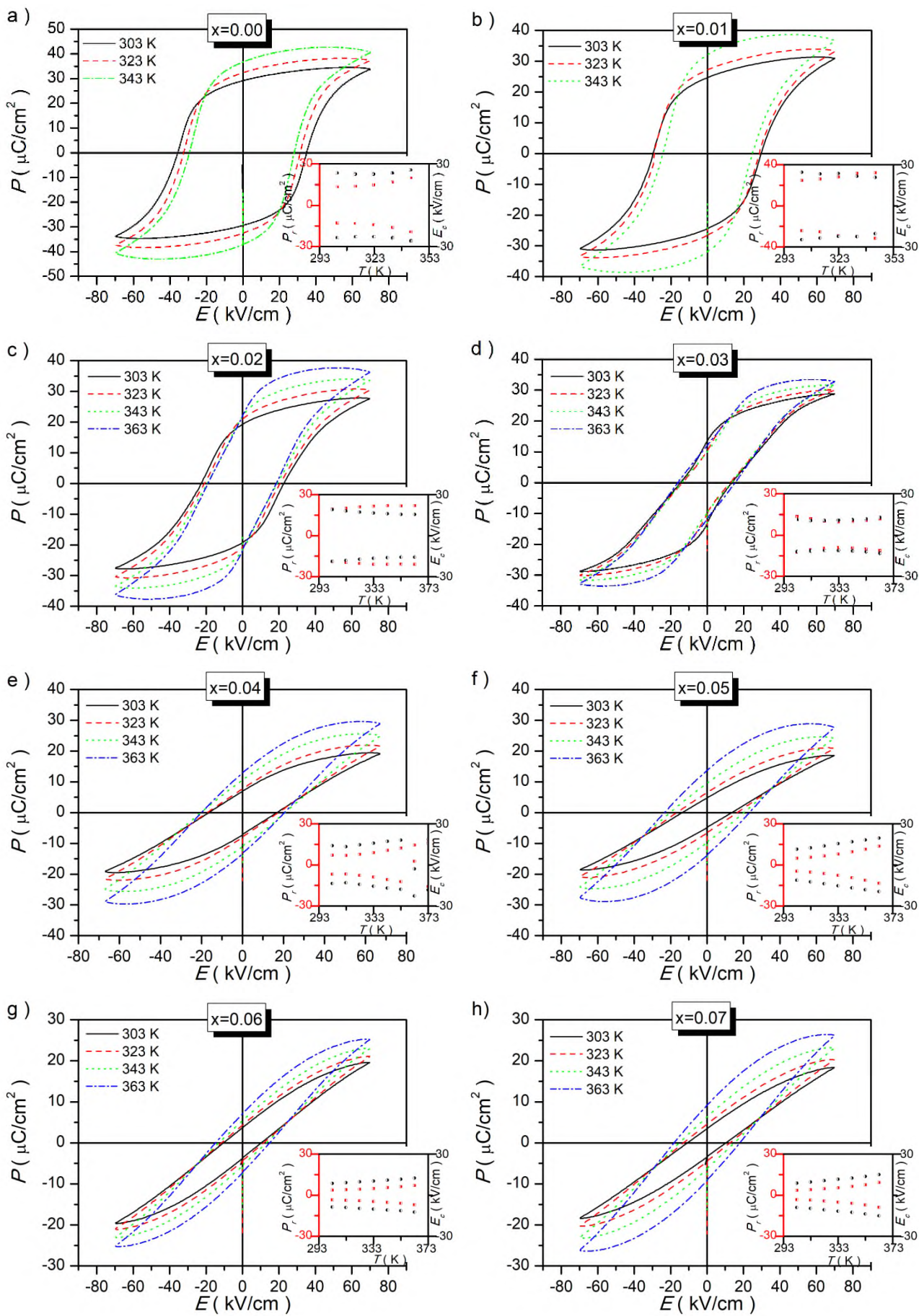


Figure S2

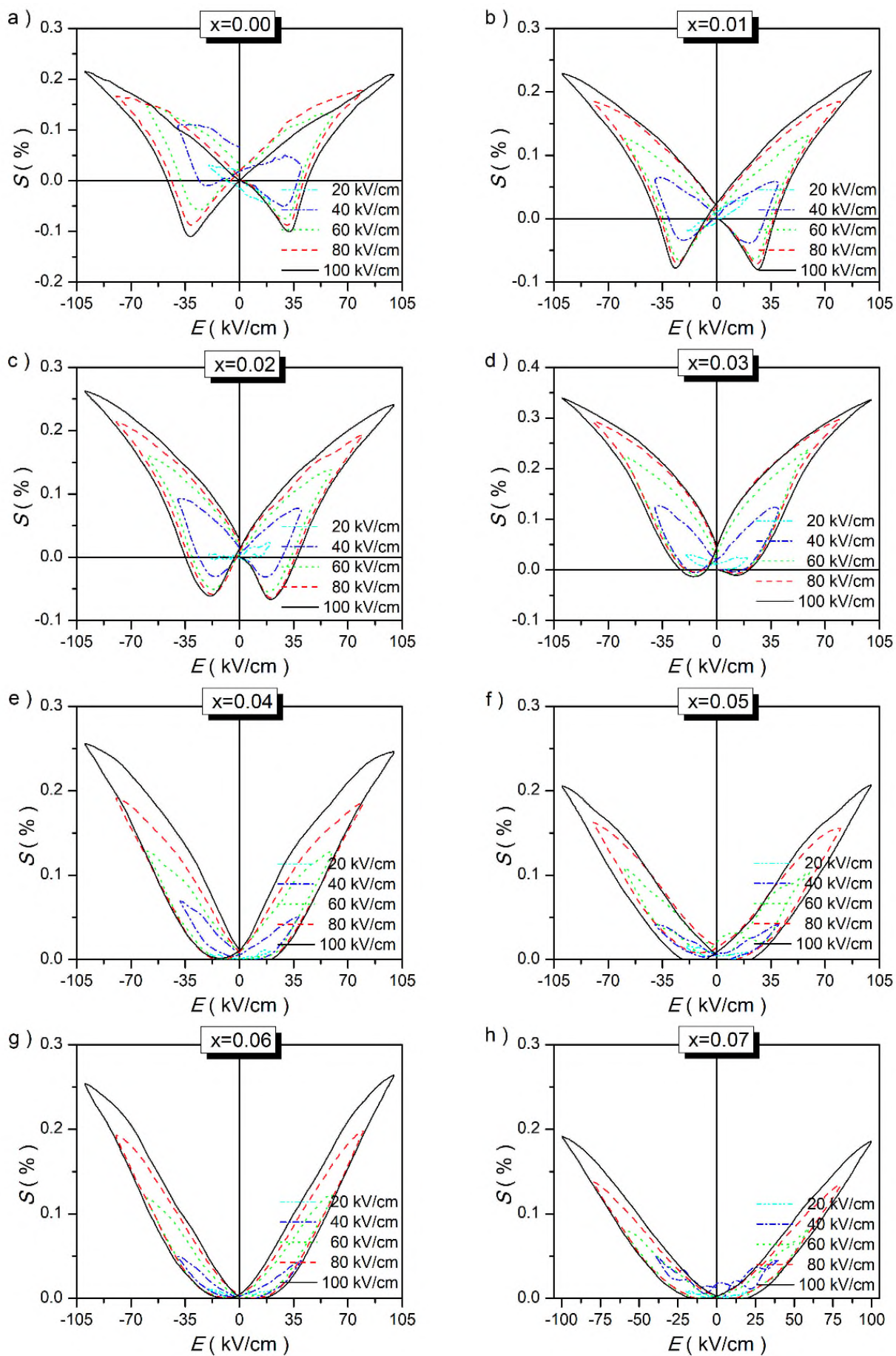


Figure S3

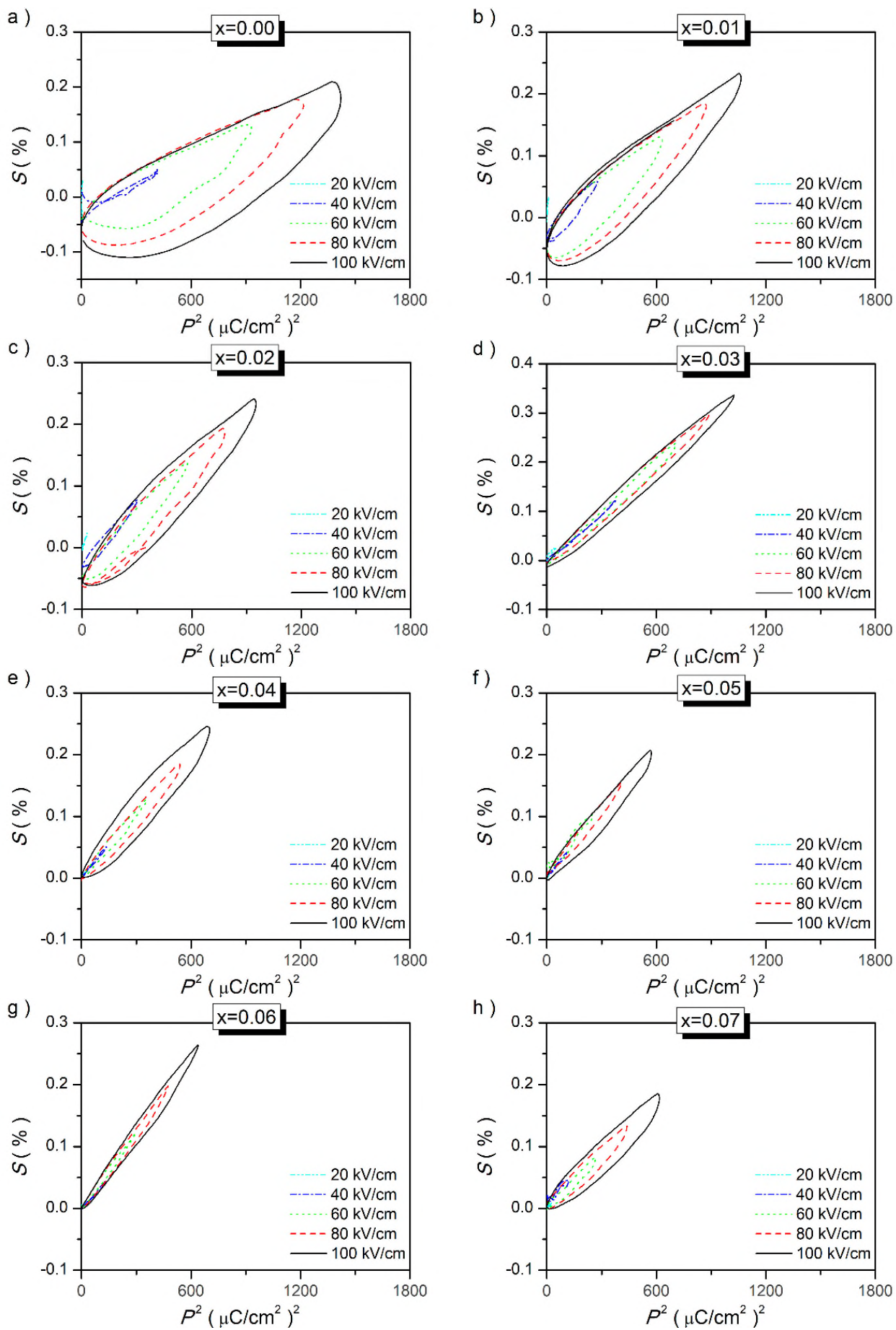


Figure S4

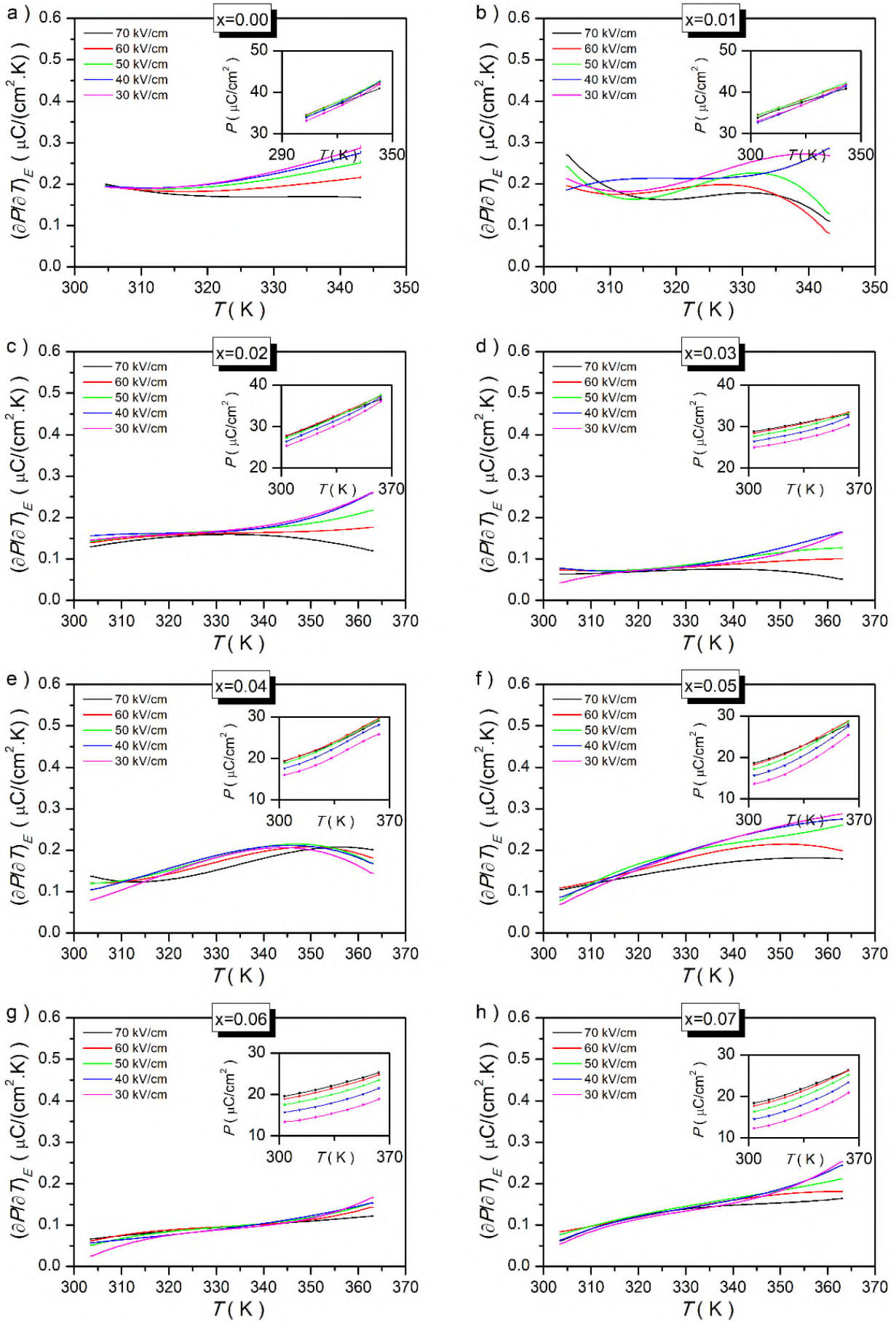


Figure S5

2019-09-23

# Phase-transition induced optimization on electrostrain, electrocaloric refrigeration and energy storage of LiNbO<sub>3</sub> doped BNT-BT ceramics

Zhang, Yueming

Elsevier

---

Zhang Y, Liang G, Tang S, et al., (2020) Phase-transition induced optimization on electrostrain, electrocaloric refrigeration and energy storage of LiNbO<sub>3</sub> doped BNT-BT ceramics. *Ceramics International*, Volume 46, Issue 2, February 2020, pp. 1343-1351

<https://doi.org/10.1016/j.ceramint.2019.09.097>

*Downloaded from CERES Research Repository, Cranfield University*